Elemental fractionation effects in high repetition rate IR femtosecond laser ablation ICP-MS analysis of glasses

Fanny Claverie, Beatriz Fernandez Garcia, Christophe Pécheyran, Joël Alexis, Olivier François Xavier Donard

Elemental fractionation effects in high repetition rate IR femtosecond laser ablation ICP-MS analysis of glasses†

Fanny Claverie,[ab] Beatriz Fernández,[a] Christophe Pécheyran,*[a] Joël Alexis[c] and Olivier F. X. Donard[a]

An IR-femtosecond laser ablation ICPMS coupling was used to investigate the influence of the high repetition rate on elemental fractionation effects for the analysis of silicate glass SRM NIST 610. First, elemental fractionation inherent to the ICP was minimised by working on wet plasma conditions which had greater tolerance to mass loading and demonstrated a higher robustness compared to dry plasma conditions. Because of the use of a narrow laser beam producing small craters (17 μm in diameter), a special arrangement of pulses was used to perform resulting craters of 100 μm diameter. The ablation strategy developed in this work consisted in a series of concentric circle trajectories ablated at high repetition rates by moving the laser beam rapidly thanks to a scanning beam device. Two scanner speeds (0.25 mm s^{-1} and 1.5 mm s^{-1}), five laser repetition rates (from 0.1 kHz to 10 kHz) and three fluence values (5 J cm^{-2}, 14 J cm^{-2}, and 25 J cm^{-2}) were investigated in detail. For this purpose, critical elemental ratios (namely $^{238}U/^{232}Th$, $^{208}Pb/^{238}U$, and $^{66}Zn/^{65}Cu$) of aerosols produced by fs-LA of silicate glass were studied to evaluate the impact of the different laser parameters on elemental fractionation. No heating zones or preferential evaporation of elements were found depending on the repetition rate employed. However, particle-size-fractionation was measured during the ablation of the sample surface, and this effect was reduced by using a high repetition rate as well as a high scanner speed which allow the dilution of the large particles coming from the surface layer with finer particles coming to deeper levels. Additionally, the ablation rate induced by the selected ablation strategy had a low influence on fractionation effects due to the high robustness of the ICP plasma and, on the other hand, fractionation indices were not particularly affected by the laser repetition rate although they could be improved by the use of high fluence values. Finally, it could be stressed that no differences on the structure of the aerosol particles collected on membrane filters were found depending on the ablation parameters.

1. Introduction

Laser ablation-inductively coupled plasma mass spectrometry (LA-ICP-MS) is currently considered as a versatile and powerful technique for the direct and element-selective analysis of solid samples. During the last year, LA-ICP-MS has become one of the most successfully applied techniques for direct major, minor, trace element and isotope ratio determinations in a wide variety of applications.[1,2] Laser ablation sampling does not require complicated sample-preparation procedures, so the risk of contamination or sample loss can be avoided. Furthermore, the focused laser beam permits the spatial characterisation of heterogeneities in solid materials with lateral and depth resolution in the low μm and nm range, respectively (*e.g.* micro-analysis, in-depth profiling, surface mapping).

However, LA-ICP-MS is still limited by the occurrence of non stoichiometric effects defined as elemental fractionation, and other possible limitations such as matrix effects, and the lack of certified reference material (CRMs) for the majority of samples of interest.[3,4] The term fractionation refers to the non-agreement between the composition of the laser-generated aerosol measured by the ICP-MS and the real elemental concentration of the bulk (*i.e.* ablated mass vapour is not chemically equal to the original sample).[5] Understanding and eliminating fractionation effects has been one of the most significant research agendas in LA sampling. Fractionation-related inaccuracies can largely be avoided if standard reference materials (SRM) of similar composition to the sample under investigation (called matrix-matched standards) are used for calibration. Unfortunately, as for many other analytical techniques, the availability of CRMs is also a serious restriction for LA-ICP-MS and, at present only a few analytical problems can be solved on the basis of matrix matching.[6,7]

All processes involved in LA-ICP-MS (the aerosol formation process, the transport of the aerosol into the ICP, and the conversion of the aerosol into ions within the ICP) may

[a]*Laboratoire de Chimie Analytique Bio-Inorganique et Environnement, Institut Pluridisciplinaire de Recherche sur l'Environnement et les Matériaux, CNRS UMR 5254, Université de Pau et des Pays de l'Adour, CNRS, Hélioparc Pau-Pyrénées, 2 Avenue du Président Angot, 64053 Pau Cedex 9, France*

[b]*Novalase SA, Z.I de la Briqueterie, 6 Impasse du bois de la Grange, 33610 Canéjan, France*

[c]*Laboratoire de Génie de Production, Ecole Nationale d'Ingénieurs de Tarbes, 47 avenue d'Azereix BP 1629, 65016 Tarbes, France. E-mail: Christophe.Pecheyran@univ-pau.fr; Fax: +33 559 407 781; Tel: +33 559 407 757*

† Presented at the 2009 European Winter Conference on Plasma Spectrochemistry, Graz, Austria, February 15–20, 2009.

potentially alter the stoichiometric composition of the laser-generated aerosol depending on the chemical and physical properties of the elements and thus, resulting in unknown contributions to elemental or isotopic fractionation effects. First, the laser-material interaction can result in ejected molten material, heat transfer beyond the ablated area, formation of large particles,[8,9] which can induce preferential evaporation of volatile elements and particle-size-related elemental composition.[10,11] The extent of these effects depends on the nature of the sample (absorption coefficient) and the characteristics of the laser (pulse duration, wavelength, and fluence). The fluence (laser energy per unit area) is the unique parameter that can be easily changed in order to improve fractionation effects, and can be considered as the major parameter to be taken into account when spatial-resolved analyses (lateral or in-depth), are of interest.[2] Several studies both for silicate glass standards and metals have recently demonstrated that the application of fluences well above the ablation threshold of the material favours the production of stoichiometric aerosols offering the possibility of accurate analysis.[3,12] Moreover, the fluence-induced effects can be minimized by the use of femtosecond (fs) laser ablation, which provides similar laser fluence with much higher irradiance.[2] The second type of laser-induced fractionation is related to the transport of the laser-generated aerosol to the ICP-MS and the failure diffusion or inertial losses of large particles to be transported to the ICP.[13] Finally, incomplete vaporisation, atomisation, and ionisation of large particles that manage to reach the ICP source can also induce fractionation effects. As it has been previously reported, large particles are more difficult to digest in the ICP compared to smaller particles[14] and can induce high positive spikes and fractionating elemental signals of the ICP-MS. Additionally, plasma loading can affect the plasma temperature decreasing its efficiency and, therefore leading to partial atomisation and, then, fractionation.[15]

The aerosol has a key role in the three different types of fractionation described for laser ablation and, therefore, knowledge about aerosol particle sizes in laser-generated aerosols and fundamental understanding of aerosol formation and particle transport are important aspects to improve LA-ICP-MS analysis. Laser-generated aerosols have been extensively characterised by using scanning electron microscope images and/or particle size distribution devices (*e.g.* low pressure impactors and differential mobility analyzers).[16–20] In an effort to improve analytical performances of LA sampling, the elimination of larger particles has been recently investigated using different tools (*e.g.* impactors,[21] filters,[22,23] separation devices,[14,24] stabilizers[25]). Nevertheless, such strategies are accompanied by a great loss of sensitivity and, therefore limit the application of LA for micro- or trace elemental analysis.

The use of ultra-short (<1 picosecond) laser pulses offers the possibility to obtain very high photon intensities with a pulse duration shorter than many fundamental time-scales, so LA on the femtosecond time-scale is predominantly non-thermal, causes less collateral damage than longer pulses, and has the potential to eliminate fractionation effects and matrix dependence. Furthermore, due to a reduced laser-material interaction, fs-La process becomes significantly less thermal,[26] providing smaller particles sizes[11] better transport efficiencies, and more stable ICP-MS signals.[27–29] Freydier *et al.*[30] showed that shorter pulses induce better analytical performances in terms of stability and accuracy and, in the case of transparent materials, the reduction of the laser wavelength was found to produce smaller particles easier to vaporise by the ICP source.[22,31] Consequently, several non-matrix matched calibrations have been successfully performed using femtosecond laser ablation systems.[32–36]

Although the influence of different laser parameters, such as the pulse duration, wavelength, spot size, and fluence, have been widely investigated for LA sampling, the effect of the laser repetition rate on fractionation is still unclear. In some cases, laser repetition rate was found to have a great influence on fractionation due to the fast overlapping of the laser pulses, which induces the heating of the sample, with no particular changes in the aerosol particle size distribution.[15,37] However on the other hand, fractionation was found to be independent of pulse repetition rate (from 4 Hz to 100 Hz),[38,39] suggesting that elemental fractionation for a 193 nm nanosecond laser is not a function of heating of the sample, since a higher pulse repetition rate leads to higher temperatures at the site of ablation. Therefore, the aim of this work is to investigate in detail the effect of the laser repetition rate on fractionation effects using a high repetition rate infrared femtosecond laser ICP-MS. For this purpose, elemental ratios of aerosols produced by fs-LA of silicate glass SRM NIST 610 were studied from moderate fluence values of 5 J cm^{-2} up to 25 J cm^{-2}, and laser repetition rate in the range of 0.1–10 kHz. The influence of the laser pulses overlapping was also studied by changing the scanner speed of the laser beam (at 0.25 mm s^{-1} and 1.5 mm s^{-1}), and, in all cases, wet and dry plasma conditions were used to compare the robustness of the ICP source. In addition, an optical profilometer was used in order to determine the topography of the ablated area, and the scanning electron microscopy (SEM) in order to obtain information about the particle size and structure of the aerosols.

2. Experimental section

2.1. Laser ablation ICP-MS system

An IR-wavelength (1030 nm) femtosecond laser ablation system (Novalase SA – France) fitted with a diode-pumped KGW-Yb laser was employed. It delivers 360 fs pulses at high repetition rate (from 1 Hz to 10 kHz) with a low energy at the sample surface in the range of 0.1 to 100 μJ. A 50 mm focal length objective was used for laser beam focusing, producing a spot size of 17 μm at the sample surface. This spot size was specified upon the $1/e^2$ criterion, assuming the lateral beam profile to be Gaussian. The laser was fitted with a galvanometric scanning beam device, allowing the fast movement of the laser beam (up to 280 mm s^{-1}) at the sample surface with high repositioning precision (±1 μm). Moreover, this laser beam movement can be synchronised with the displacement of the sample, *via* two motorised XY stages, in order to perform complex trajectories. Features and further details of the applied laser ablation system are described elsewhere.[29]

An Elan DRC II (Perkin Elmer) was used for ICPMS measurements. Helium was chosen as carrier gas in the ablation cell, and a Y-piece connection was installed at the torch inlet of the ICP-MS allowing the mixing of the laser-generated aerosol with an additional argon flow used to reach the optimal

conditions in terms of sample introduction into the ICP. Two different plasma configurations (wet and dry) were studied. Wet plasma conditions were obtained with the dual introduction of the laser-generated aerosol and a liquid aerosol obtained by nebulising a nitric solution (1% in MilliQ water) *via* the pneumatic nebulizer. The additional argon flow was thus introduced *via* a conical spray nebulizer fitted in a cyclonic spray chamber. Dry plasma conditions were obtained by directly connecting the additional argon flow to the Y-piece, without passing through the pneumatic nebulizer. For both configurations, ICPMS tuning was accomplished ablating a 100-μm wide lane on the silicate glass SRM NIST 612 and taking into account sensitivity, background intensity, and the $^{238}U/^{232}Th$ signal ratio that should be close to 1 to ensure a low fractionation effect due to the ICP ionisation efficiency. Table 1 summarises the operating conditions used for the laser ablation and the ICPMS systems.

2.2. Ablation strategies

The main problem related to the use of a low-energy laser is the necessity of using a narrow laser beam in order to ensure a fluence above the ablation threshold. It results in a small ablated volume which is suitable for microanalysis but provides low signal sensitivity. As an alternative, the LA-ICPMS signal sensitivity can be recovered by increasing the sample removal rate and the sample ablated volume. The sample ablated volume can be drastically enhanced by using the fast scanning beam device of the laser in combination with high repetition rates. This arrangement allows performing complex ablation trajectories extending the sample surface impacted by the laser. This unique characteristic of the laser has been already successfully investigated to increase LA-ICPMS sensitivity[40,41] (by ablating large scans or craters) and to perform direct in-cell isotope dilution analysis[42] (by ablating quasi-simultaneously two different samples).

Table 1 Operating conditions of the LA-ICPMS system

ICP-MS Elan DRC II	Wet Plasma Conditions	Dry Plasma Conditions
Argon flow rates:		
• Plasma gas	15.0 L min^{-1}	15.0 L min^{-1}
• Auxiliary gas	1.10 L min^{-1}	1.10 L min^{-1}
• Nebulizer gas	0.6 L min^{-1}	0.6 L min^{-1}
Water uptake rate	64 μL min^{-1}	0 μL min^{-1}
ICP RF Power	1400 W	1470 W
Dwell time	10 ms	
Isotopes	^{7}Li, ^{23}Na, ^{27}Al, ^{29}Si, ^{42}Ca, ^{43}Ca, ^{55}Mn, ^{57}Fe, ^{61}Ni, ^{65}Cu, ^{66}Zn, ^{75}As, ^{89}Y, ^{111}Cd, ^{121}Sb, ^{133}Cs, ^{139}La, ^{165}Ho, ^{169}Tm, ^{181}Ta, ^{208}Pb, ^{209}Bi, ^{232}Th, ^{238}U	

Laser Ablation System	ALFAMET (Novalase SA)
Wavelength	1030 nm
Pulse duration	360 fs
Repetition rate	From 0.1 kHz to 10 kHz
Fluence	From 5 J cm^{-2} to 25 J cm^{-2}
Carrier gas flow rate	0.65 L min^{-1} of He
Ablated area:	
• Crater mode	100 μm in diameter (6 concentric circles)

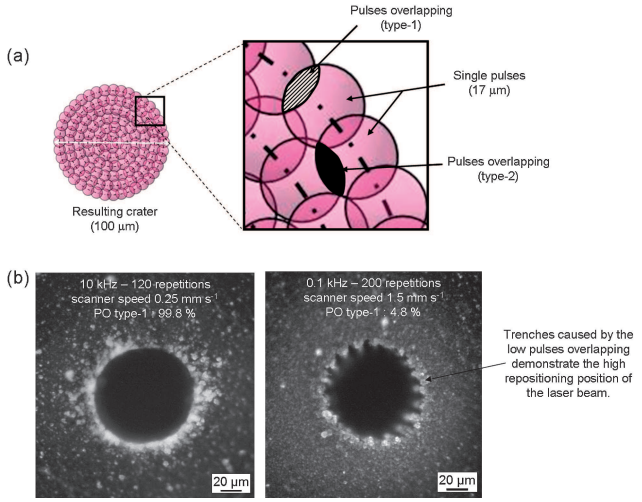

Fig. 1 Schematic of laser ablation strategy employed and its resulting crater. a) Illustration of the Pulses Overlapping (PO): type-1 refers to the laser pulses overlapping on a same concentric circle, and type-2 refers to the laser pulses overlapping between different concentric circles. b) Resulting craters obtained, on NIST 610, for the highest and the lowest pulses overlapping obtained at 10 kHz and 0.25 mm s^{-1} scanner speed and 0.1 kHz and 1.5 mm s^{-1} scanner speed respectively. As it can be seen, some particle deposits were found around each craters.

In the present work, in order to produce a well-defined crater of desired diameter (see Fig.1), the ablation strategy is based on the virtual increasing of the laser beam spot size (17 μm) by ablating the sample according to concentric circles trajectories. In our case, a set of six concentric circles uniformly distributed (Ø 83μm, Ø 70.4 μm, Ø 57.8 μm, Ø 45.2 μm, Ø 32.6 μm and Ø 17 μm) were used to define a laser ablation crater of 100-μm diameter. This series of six concentric circles trajectories was repeated 20 and 125 times for 0.25 mm s^{-1} and 1.5 mm s^{-1} respectively, resulting in the final crater. In these conditions, the resulting crater is obtained by a succession of small craters (Ø 17 μm) partially overlapped. Two different types of laser pulses overlapping can be distinguished in the resulted crater: the first one (denoted as type-1), describes the spatial overlapping of small pulses belonging to a given concentric circle (Fig.1a, white part striped), and the second one (denoted as type-2), describes the spatial overlapping of small pulses belonging to consecutive concentric circles (Fig.1a, black part). Then, for a given crater diameter, the overlapping of the laser pulses depends on the laser repetition rate, the speed rate of the laser beam, and the number of concentric circles.

It should be highlighted that the advantage of using this complex ablation strategy is the increase of the ablated area without changing the fluence of the laser. Therefore, in order to keep the same overlapping conditions for all the repetition rates investigated, the scanner speed had to be increased with the repetition rate. Two moderate scanner speed rates of the laser beam (0.25 mm s^{-1} and 1.5 mm s^{-1}), five different repetition rates (from 0.1 kHz to 10 kHz), and three fluence values (5 J cm^{-2}, 14 J cm^{-2}, and 25 J cm^{-2}) were studied as regards to elemental fractionation. Higher scanner speeds could not be investigated in the scope of this study since, at high repetition rate, a fast sample removal was produced. The ablation process duration was only

Table 2 Experimental parameters investigated for fs-LA-ICPMS analyses and resulted laser pulses overlapping for each of them

	Scanner Speed (mm s^{-1})	Laser Pulses Overlapping (%) [type-1/type-2][a]	Number of pulses (6 concentric circles)	Repetition of the 6 concentric circles	Fluence (J cm^{-2})
0.1 kHz	0.25	81.3/15.2	388 in 3.88 s	20	5, 14, and 25
	1.5	4.8/15.2	64 in 0.64 s	125	
0.3 kHz	0.25	93.8/15.2	1164 in 3.88 s	20	5, 14, and 25
	1.5	63.1/15.2	194 in 0.64 s	125	
1 kHz	0.25	98.1/15.2	3883 in 3.88 s	20	5, 14, and 25
	1.5	88.8/15.2	647 in 0.64 s	125	
5 kHz	0.25	99.6/15.2	19415 in 3.88 s	20	5, 14, and 25
	1.5	97.8/15.2	3235 in 0.64 s	125	
10 kHz	0.25	99.8/15.2	38830 in 3.88 s	20	5, and 14
	1.5	98.9/15.2	6471 in 0.64 s	125	

[a] type-1: spatial overlapping of laser pulses belonging to a given concentric circle, type-2: spatial overlapping of laser pulses belonging to consecutive concentric circles.

for a few seconds (<15 s), which was considered as insufficient to assess the elemental fractionation processes with a quadrupole ICPMS. The ablation conditions used as well as the corresponding laser pulses overlapping are summarised in Table 2.

2.3. Scanning electron microscopy

The laser-generated aerosol was visualised using a scanning electron microscope (field emission scanning JEOL 7000F, JEOL Ltd., Japan) operated at 5 kV. Aerosol particles were collected on nucleopore polycarbonate track-etch membrane filters with a pore size of 200 nm (Whatman Inc., USA), which were placed in the transfer tube approximately 1 m behind the ablation cell. The membrane filters were stuck on SEM-mounts using a conducting carbon tape and, subsequently metallised during 4 min with a SEM coating E5000 (Polaron Equipment LTD) at intensity levels in the range of 16–18 mA under nitrogen atmosphere (2.37 10^{-4} atm). Palladium was used as conductive surface coating in order to remove artefacts.

2.4. Ablation topography

Penetration depths and profiles of the ablated area were performed by using an optical surface profilometer Micromesure CHR150 (STIL Society, Aix en Provence, France). Such a profilometer is equipped with a high-resolution optical sensor with a field depth of 1000 μm and a lateral axis resolution of 0.156 μm. Data were acquired by the SurfaceMap software and treated with the MountainMap Universal software.

3. Results and discussion

It is now well established that most of elemental fractionation effects come from complex thermodynamic processes taking place during the laser-sample interaction and, later on, into the plasma of the ICP itself. Preferential evaporation of some elements at the sample surface, atomisation efficiency of particles as well as ionisation efficiency of the elements in the ICP are the main phenomena that explain elemental fractionation.[1,43] Three signal ratios, namely $^{238}U/^{232}Th$, $^{66}Zn/^{65}Cu$ and $^{208}Pb/^{238}U$ have been recently proposed [15,22,36,44] in order to assign the nature and the origin of elemental fractionation. Different studies have shown that the $^{238}U/^{232}Th$ ratio of a homogenous sample is a powerful tool to assess particle-size-related elemental fractionation.[10,14,22,24] The $^{238}U/^{232}Th$ ratio evolves in the same way that the particle size distribution,[22] and thus, the larger the particles, the higher the signal ratio. The $^{66}Zn/^{65}Cu$ ratio is more related to the ionisation efficiency and the temperature of the plasma.[15] The $^{66}Zn/^{65}Cu$ ratio represents a critical elemental system due to the high ionisation energies of these elements which differ by 18% (E_{Zn} = 906 kJ mol^{-1} and E_{Cu} = 745 kJ mol^{-1}). Zn is more difficult to ionise than Cu and, therefore, is significantly more affected by changes in plasma temperature. Finally, the $^{208}Pb/^{238}U$ ratio can be used as an evidence of fractionation through the preferential evaporation of volatile elements in the carrier gas over the course of the ablation.[36] During the laser ablation, with the increase of the crater depth, the ratio of a volatile element (*e.g.* Pb) to a refractory element (*e.g.* U) evolves from its real ratio to significantly higher values for nanosecond ablation.[32] Therefore, in the present work these three elemental ratios ($^{238}U/^{232}Th$, $^{66}Zn/^{65}Cu$ and $^{208}Pb/^{238}U$) were carefully investigated in order to better understand the nature of elemental fractionation occurring in infrared femtosecond laser ablation ICPMS analyses.

3.1. Effect of the ICPMS plasma conditions on the elemental fractionation

In a recent study, O'Connor *et al.*[45] demonstrated the stronger robustness of the ICP operated in wet plasma conditions and its greater tolerance to mass loading compared to the more conventional dry plasma conditions used in LA-ICPMS, indicating that ICP related elemental fractionation is minimised under wet plasma conditions. However, such a study was just focused on 266 nm nanosecond laser pulses. One of the aims of our study was to verify whether or not similar conclusions could be stated in the case of infrared femtosecond pulses. Thus, the $^{238}U/^{232}Th$, $^{66}Zn/^{65}Cu$, and $^{208}Pb/^{238}U$ ratios were studied in wet (where 64 μL min^{-1} of water were introduced into the plasma) and dry plasma conditions for each laser ablation condition investigated (see Table 2): repetition rate 0.1 kHz, 0.3 kHz, 1 kHz, 5 kHz, and 10 kHz, fluence value 5 J cm^{-2}, 14 J cm^{-2}, and 25 J cm^{-2}, and scanner speed: 0.25 mm s^{-1} and 1.5 mm s^{-1}. These ratios were calculated from the top of the ICP-MS signal and during 15 seconds.

Table 3 presents the deviation of the $^{238}U/^{232}Th$, $^{66}Zn/^{65}Cu$, and $^{208}Pb/^{238}U$ elemental ratios relative to the dry plasma conditions. No significant changes were observed for the $^{208}Pb/^{238}U$ ratio using different laser ablation conditions, indicating that the signal ratio was also not particularly affected by the ICP conditions tested (wet and dry plasma conditions). As the $^{208}Pb/^{238}U$ ratio is supposed to mainly describe preferential evaporation likely to occur during laser-sample interaction, no drastic changes should be expected by modifying the ICP conditions. Pb and U have relatively low ionisation potentials and, consequently, are affected to a lesser extent by changes of the ICP temperature. The $^{238}U/^{232}Th$ ratio was also found to be quite similar for all experimental conditions investigated. This might indicate that wet or dry plasma conditions do not modify significantly the atomisation efficiency of the particles produced under the selected laser ablation conditions. It should be stated that the ICPMS was tuned for both plasma conditions in order to achieve a value for the $^{238}U/^{232}Th$ ratio close to 1, which is the true value generally accepted for the SRM NIST 612. Therefore, the tuning of the ICPMS was performed with a different sample (SRM NIST 612 *versus* SRM NIST 610) and laser ablation strategy (raster *versus* crater ablation mode) which clearly demonstrates that robust atomisation conditions were used. On the other hand, it can be highlighted that a higher plasma power had to be applied for dry plasma conditions compared to wet plasma (1470 W *versus* 1400 W) to reach, in both cases, the optimum $^{238}U/^{232}Th$ ratio (Table 1).

In contrast to the $^{238}U/^{232}Th$ and $^{208}Pb/^{238}U$ ratios, the $^{66}Zn/^{65}Cu$ ratio was intensively affected by the plasma conditions. In all cases, the two different configurations investigated showed an increase of the $^{66}Zn/^{65}Cu$ ratio from dry to wet plasma, this increase in the range of 32–55% being dependent on the laser ablation parameters (repetition rate, fluence, and scanner speed). This change in the $^{66}Zn/^{65}Cu$ ratio indicates that Zn is more effectively ionised into the ICP under wet plasma conditions and highlights either a higher plasma temperature or a change of the vaporization place within the plasma of the ICP. The addition of water might allow the small particles to grow. These particles would therefore penetrate more deeply into the plasma. The diffusion into the plasma of small particles prone to Zn-enrichment (in brass[11] and glass[19]) might then be reduced which would induce higher Zn signals and thus higher Zn/Cu ratios. On the other hand, as it has been previously reported by Koch *et al.*,[15] the estimation of plasma temperature changes from dry to wet plasma conditions was calculated using the simplified Saha equation. For this purpose, ^{66}Zn and ^{65}Cu were used as thermometric elements because of their different ionisation potentials, and the $^{66}Zn/^{65}Cu$ response ratio was recorded for each ablation under wet and dry plasma conditions. Experimental results showed that the temperature of the plasma in wet conditions is from 698 K to 1112 K higher compared to dry plasma conditions depending on the ablation parameters employed. The evaluation of the robustness of the plasma depending on the aerosol introduced (*e.g.* wet, partially desolvated and dry) was widely studied during the last few decades, for inductively coupled plasmas. High speed images of the ICP showed that some particles were incompletely vaporised on each condition,[46] and different opinions disagree on the influence of water loading and desolvation,[47] which results in an increase or a decrease of the temperature and the electron density. It seems that the ICPMS conditions employed are of greater importance.[48] When suitable operating conditions are used (*i.e.* a robust plasma with a high RF power and a low carrier gas flow rate), the presence of water could play a beneficial role.[47] Water is supposed to buffer the plasma against the effects caused by the introduction of particles, dominating the plasma loading and, therefore, small perturbations induced by the ablated particles can be negligible. In contrast, if these suitable ICPMS conditions are not reached, the water consumes an important part of the energy available on the plasma in order to be desolvated and, thus reduces the energy available for the particles. In certain conditions, water has been found to have a positive effect on

Table 3 $^{238}U/^{232}Th$, $^{208}Pb/^{238}U$, and $^{66}Zn/^{65}Cu$ ratios obtained by IR-fs-LA-ICPMS under wet and dry plasma conditions. Deviation values are referred to the signal ratios obtained on dry plasma conditions. The precision of the signal ratios measurements was calculated based on 1S-standard deviation from the mean of three replicates, being the precision in the range of 0.1–13%

	$^{238}U/^{232}Th$		$^{208}Pb/^{238}U$		$^{66}Zn/^{65}Cu$	
	0.25 mm s^{-1}	1.5 mm s^{-1}	0.25 mm s^{-1}	1.5 mm s^{-1}	0.25 mm s^{-1}	1.5 mm s^{-1}
25 J cm^{-2}						
0.1 kHz	−0.4%	0.5%	−8%	−5%	33%	35%
0.3 kHz	2.4%	4.4%	−10%	−9%	36%	35%
1 kHz	0.2%	2.6%	−7%	−7%	39%	38%
5 kHz	2.0%	3.4%	−9%	−2%	39%	39%
10 kHz	—	—	—	—	—	—
14 J cm^{-2}						
0.1 kHz	−0.9%	−3.4%	−2%	−4%	35%	36%
0.3 kHz	−3.4%	0.6%	−8%	−8%	34%	32%
1 kHz	4.0%	3.7%	−8%	−5%	36%	33%
5 kHz	−2.2%	3.7%	5%	−5%	51%	43%
10 kHz	−1.3%	4.1%	11%	−10%	55%	32%
5 J cm^{-2}						
0.1 kHz	−4.7%	−7.3%	−7%	1%	39%	33%
0.3 kHz	−8.8%	−4.4%	−6%	−5%	32%	32%
1 kHz	−4.0%	0.6%	−11%	−7%	38%	33%
5 kHz	−0.7%	−4.0%	−3%	−4%	43%	35%
10 kHz	−2.9%	−1.2%	1%	−4%	52%	49%

signal sensitivity due to hydrogen brought by water that increases the electron density.[49] The positive effect of the hydrogen was also demonstrated by Guillong and Heinrich[50] who found enhanced sensitivity for most of the 47 elements investigated when introducing a few millilitres per minute of hydrogen to the carrier gas. In this sense, Günther and Heinrich[51] showed an increase of signal sensitivity when introducing moist argon instead of dry argon with the helium carrier gas. However, this was accompanied by higher polyatomic interferences increasing the background especially in the low mass region. Similarly, sensitivity was enhanced in our wet plasma conditions for all elements and higher background intensities were observed for ^{29}Si, ^{42}Ca, ^{55}Mn and ^{58}Fe.

Furthermore, up to now, the major publications have investigated wet plasma conditions as solution nebulisation, and dry plasma as desolvated aerosol or dry aerosol coming from the laser ablation process, and only a few articles have dealt with wet plasma as a mixture of nebulisation and laser ablation, as well as dry plasma as a laser ablation aerosol only. O'Connor *et al.*[45] have recently demonstrated the greater robustness of the plasma on wet conditions for nanosecond laser ablation as mentioned above. The improvement on particle size distribution inherent to femtosecond laser ablation does not overcome the poor robustness of dry plasma conditions, taking into account that our results showed the same conclusions even with a higher radio-frequency plasma power for dry conditions. It could be partly due to the high ablation rate performed with our special arrangement of the scanner beam and the high repetition rate which induce a high sample removal in a short time.

Therefore, since a higher temperature of the plasma and a greater robustness of the ICP source were obtained, such conditions were selected for all the subsequent measurements in order to ensure a lower ICP fractionation.

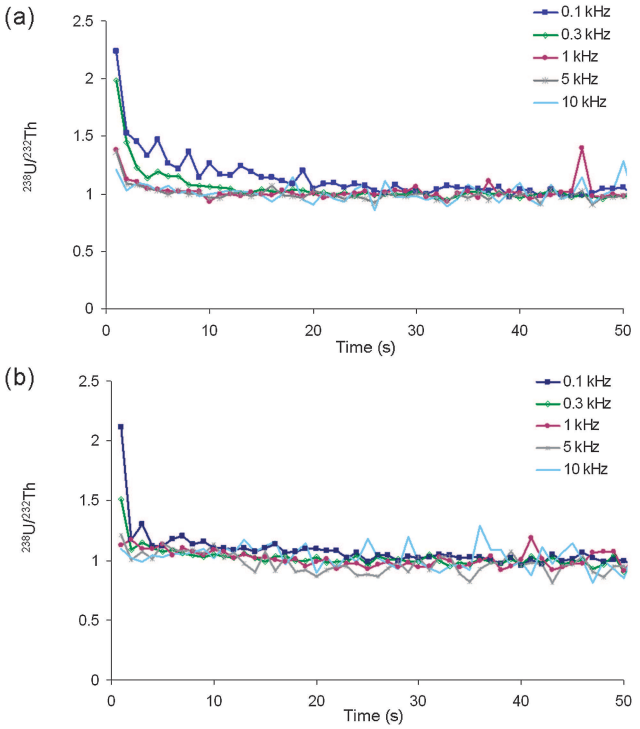

Fig. 2 Evolution of the ^{238}U/^{232}Th ratio obtained during fs-LA-ICPMS analysis of SRM NIST610. Selected experimental conditions: six concentric circles repeated 200 times (resulting crater diameter 100 μm); fluence 14 J cm^{-2}; laser repetition rate in the range of 0.1–10 kHz. In order to better visualise signal variation, each point represents an averaged ratio recorded during one second. Standard deviation values are calculated from the mean of three analyses, being the precision below 5% in all cases. a) scanner speed of 1.5 mm s^{-1}, b) scanner speed of 0.25 mm s^{-1}.

3.2. Particle-size-related fractionation

The laser ablation system used in this work differs drastically from those previously reported in the literature for LA-ICP-MS analysis due to its unique capacity to make craters by combining a high repetition rate (<10 kHz) with a fast movement of the laser beam at the surface of the sample. Nevertheless, this unusual ability could suggest some questions about the particle size distribution and the related elemental fractionation. For instance, may a high repetition rate undergo particle-size-related fractionation? And, may the scanner speed influence particle-size-related fractionation if the small craters overlap insufficiently provoking the ejection of micron-size debris?

As described above, the particle-size-related fractionation can be assessed by studying the ^{238}U/^{232}Th ratio over the course of the ablation. Thus, in the present section, the effect of the scanner speed was studied as regards to particle-size-related fractionation using different repetition rates but maintaining a constant fluence value of 14 J cm^{-2}. First, Fig. 2a shows the ^{238}U/^{232}Th ratio obtained by fs-LA-ICPMS from the mean of three replicates performed with a scanner speed of 1.5 mm s^{-1}. As it can be seen, using a laser repetition rate of 0.1 kHz, the first pulses performed showed a strong particle size fractionation in comparison with those obtained for 1 kHz and 5 kHz (the ^{238}U/^{232}Th ratio changed from 1.4 up to 2.3). However, the fractionation observed during the first pulses could be significantly reduced by increasing the repetition rate up to 10 kHz (in this case, the ^{238}U/^{232}Th ratio was in the order of 1.2). Guillong *et al.*[22] reported the production of large particles when the ablation is performed at the surface of the material and the production of smaller particles as the crater depth increases. Therefore, particle-size-related fractionation could be different depending on the analysis time (*i.e.* depending on the ablation depth) and, thus, understanding how our craters are drilled, in terms of mass sample removal rate over the time is of great importance.

Using a scanner speed of 1.5 mm s^{-1}, the laser pulses overlapping (type-1) varies drastically as a function of the laser repetition rate in the range of 4.8% to 98.9% and, consequently affects the crater depth as a function of time. Fig. 3 shows the crater shapes obtained in the glass sample after fs-LA-ICPMS analysis using a scanner speed of 1.5 mm s^{-1} and different repetition rates (0.1 kHz, 1 kHz and 10 kHz).

As can clearly be seen, the removal rate increased with the laser repetition rate: the higher the repetition rate, the deeper the depth of the analysis. For instance, after 3.2 s of ablation, the crater depth was about 5 μm at 0.1 kHz whereas at 10 kHz this was about 90 μm demonstrating that the laser beam spent much more time ablating the surface layer which is prone to produce large particles at low repetition rate compared to higher repetition rates. This effect could explain, at least partly, the reason why the

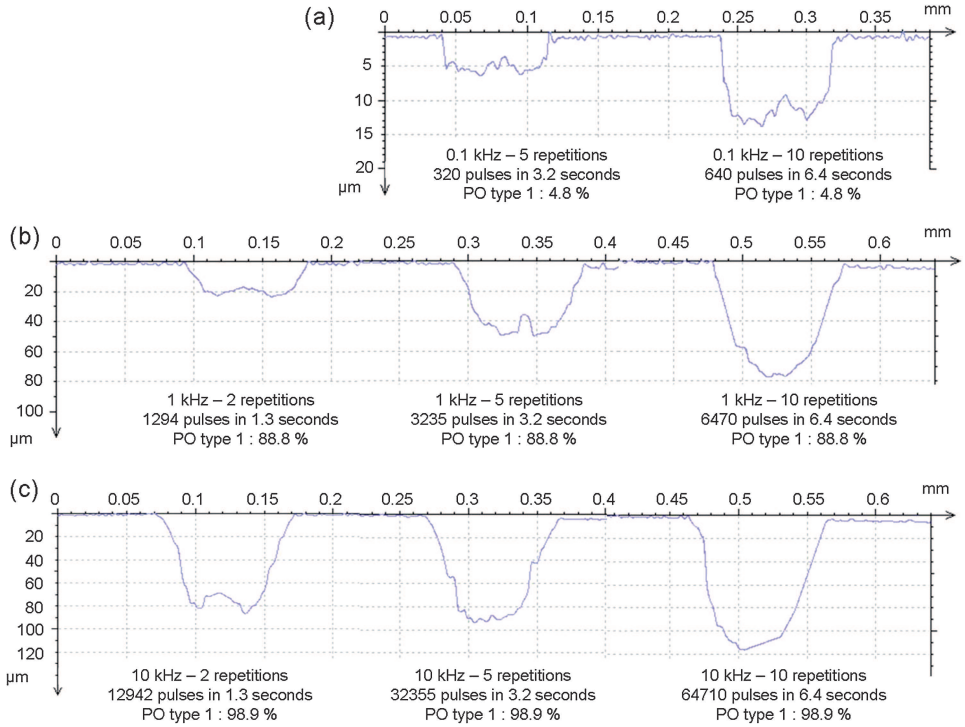

Fig. 3 Ablation topography of craters obtained at (a) 0.1 kHz, (b) 1 kHz and (c) 10 kHz with the 6 concentric circles strategy repeated 2, 5 and 10 times (from the left to the right) at 1.5 mm s^{-1} scanner speed and 14 J cm^{-2} fluence value. The Pulses Overlapping (PO) type-1 as well as the time duration of the ablation and the number of pulses performed during the ablation are noted below each graph. At 0.1 kHz for the ablation repeated twice, the profilometer was not able to measure the low depth of the ablation.

$^{238}U/^{232}Th$ ratio reached more rapidly the true value at high repetition rates.

In order to verify whether or not the particle size distribution of the laser-generated aerosol produced at high repetition rate is significantly different to that produced at low repetition rate, aerosol particles collected on polycarbonate filters were examined by SEM. Fig. 4 shows typical SEM images of the aerosol particles obtained for the glass SRM NIST 610 after fs-LA analysis, using two laser repetition rates (0.1 kHz and 10 kHz) and two scanner speeds (0.25 mm s^{-1} and 1.5 mm s^{-1}). These images cannot be used to provide quantitative information about particle size distribution due to the nonuniform distribution of particles on filter surfaces, but reveal the shape and texture of the particles, which provides crucial information about particle formation processes. As can be seen, linear agglomerates of nanometric particles and a few molten spherical particles were found in all cases. Similar observations are reported in the literature under nanosecond (193 nm) and femtosecond conditions when ablating glasses or metals.[17,18,52,53] The SEM pictures also revealed that aerosols produced in this work are very similar in terms of size and structure to those produced by 193 nm nanosecond laser ablation of the same glass material as shown in.[18] This shows that deep UV nanosecond laser can provide similar particles than IR femtosecond laser. Furthermore, both, the structure and the number of particles were very similar for the two repetition rates investigated and, therefore, it can be stressed that the laser repetition rate itself might not play a major role in the formation of thin or large particles for fs-LA analysis of glass samples since no significant differences were found between the SEM images. Thus, the biased $^{238}U/^{232}Th$ ratio measured in the early stage of the ablation seems to be governed by the speed to which craters are drilled, although this does not preclude the ejection of thick particles at 10 kHz when the first layers of the sample are ablated. As mentioned above, the $^{238}U/^{232}Th$ ratios of 1.2 were still recorded during the first seconds of the analysis at high repetition rate. Indeed, even for a short given period of time (*e.g.* at the second scale), the ablation rate and, then, the speed of

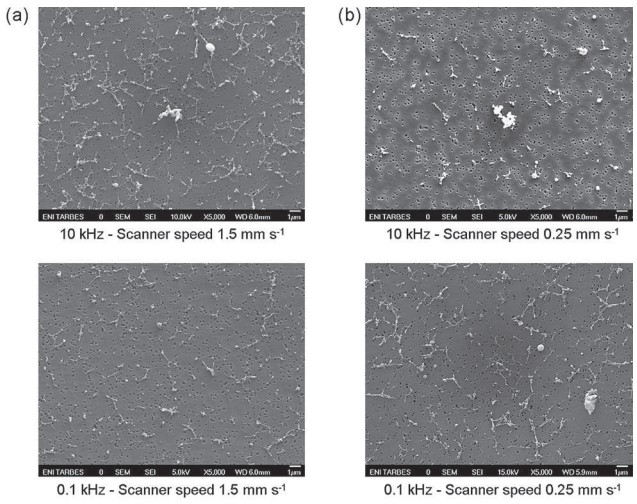

Fig. 4 SEM images of the collected aerosol produced at 14 J cm^{-2} a) scanner speed of 1.5 mm s^{-1} at 10 kHz (above) and 0.1 kHz (below) b) scanner speed of 0.25 mm s^{-1} at 10 kHz (above) and 0.1 kHz (below).

drilling were so fast in these conditions, that the biased $^{238}U/^{232}Th$ ratio corresponding to the first ejected thick particles was lowered by the large occurrence of very small particles generated below the initial sample surface. In other words, the thick particles were strongly diluted with the thin particles, which likely explain the lower $^{238}U/^{232}Th$ ratios obtained in the first seconds of the ablation when high repetition rates are used.

On the other hand, when the scanner speed was lowered to 0.25 mm s^{-1}, the $^{238}U/^{232}Th$ ratios followed the same trend as those obtained for a scanner speed of 1.5 mm s^{-1}. As it can be seen from Fig. 2b, for low repetition rates, the true value of the $^{238}U/^{232}Th$ ratio was obtained earlier compared to the ablations operated with a scanner speed of 1.5 mm s^{-1}. The beginning of the ablation showed lower $^{238}U/^{232}Th$ ratios than those obtained at 1.5 mm s^{-1} particularly for the lowest repetition rates (*e.g.* at 0.1 kHz the ratio changed from 2 at 1.5 mm s^{-1} to 1.7 at 0.25 mm s^{-1}). This change could be explained by the origin of the particles. In contrast to ablations performed at 1.5 mm s^{-1}, where the laser ablated only the surface layer of the sample over a few seconds, at 0.25 mm s^{-1} the laser beam ablated the same zone over more time and, thus, the depth of the analysis was higher. The laser-generated aerosol obtained during the first seconds of the analysis is then composed of a mixture of surface ablated particles and particles coming from the deep layer (prone to be the smallest), that could explain the lower $^{238}U/^{232}Th$ ratios obtained at the beginning of the ablation. This is most visible at low repetition rates due to the overlapping of the laser pulses (type-1) which was much more different. For example, at 0.1 kHz, this parameter increased from 4.8% at 1.5 mm s^{-1} to 81.3% at 0.25 mm s^{-1} compared to ablations performed at 10 kHz where the pulses overlapping (type-1) were almost similar (98.9% and 99.8% at 0.25 mm s^{-1} and 1.5 mm s^{-1} respectively).

Additionally, it could be observed that the structure and the number of particles obtained in SEM images for the laser-generated aerosol were very similar for the two repetition rates and the two scanner speeds investigated (Fig 4). Fig. 4b show the morphology of the collected particles using a scanner speed of 0.25 mm s^{-1} (both for 0.1 kHz and 10 kHz laser repetition rates) and, it can be highlighted that it was quite similar in comparison with that obtained using a scanner speed of 1.5 mm s^{-1} (Fig 4a). Therefore, on the basis of this observation, it could be concluded that the laser pulses overlapping does not affect the size of the ejected particles in the analysis of glass samples.

3.3 Preferential evaporation and plasma loading effects

As mentioned above, the ablation strategy employed in the present work is based on the overlapping of laser pulses delivered very rapidly at the sample surface. The laser repetition rate governs directly the ablation rate as a function of time and, consequently, might be related to elemental fractionation due to plasma loading effects. Indeed, Kroslakova *et al.*[54] have reported significant changes of element/Ca ratio depending on the mass load of the ICP for laser ablation of glass samples. On the other hand, the combination of laser ablation at high repetition rates and strong overlapping might also suggest questions about the occurrence of heating zones and, therefore, about the preferential evaporation of volatile elements due to the short period of time between one pulse to the following one (from 10 ms to 0.1 ms in this study). As it can be seen in Fig. 4, evidences of thermal effects were found in some of the thin collected particles presenting a spherical shape likely due to melting and cooling processes. However, the different crater shapes presented in Fig. 3 did not show, in any case the presence of molten crater rims which could indicate melting processes during laser ablation analyses.

In order to assess if infrared femtosecond pulses delivered at a high repetition rate induce elemental fractionation effects due to preferential evaporation, the $^{208}Pb/^{238}U$ ratio was studied for laser repetition rates ranging from 0.1 kHz to 10 kHz maintaining a constant fluence value of 14 J cm^{-2}. As it can be seen from Fig 5a, experimental results obtained for both scanner speeds investigated (1.5 mm s^{-1} and 0.25 mm s^{-1}) showed a slight negative deviation of the $^{208}Pb/^{238}U$ ratios as a function of the laser repetition rate. However such a deviation was no significant and did not exceed 11% from 0.1 kHz to 10 kHz. The $^{208}Pb/^{238}U$ ratio is supposed to mainly describe preferential evaporation occurring during laser-material interaction and thus, severe surface heating induced by high repetition rates and pulse overlapping should induce an increase of the $^{208}Pb/^{238}U$ ratio, taking into account that lead has the lowest boiling point temperature and the lowest melting point temperature compared to uranium. In contrast to this theory, the opposite trend was observed suggesting that high repetition rates and strong pulse overlapping did not induce detectable preferential evaporation. Although it is not possible to conclude undoubtedly that repetition rate and pulses overlapping have negligible effect on the occurrence of this type of fractionation, it is clear that stronger effects dominate

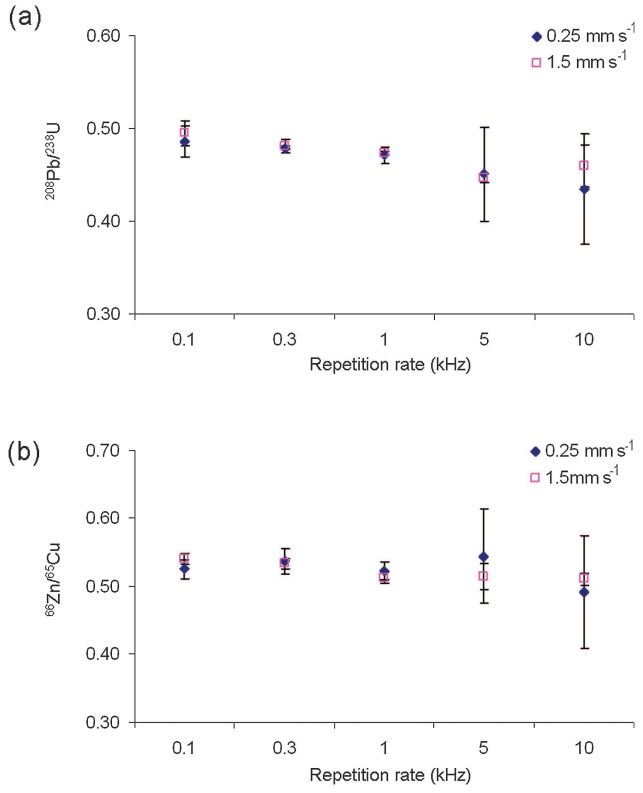

Fig. 5 Evolution of the (a) $^{208}Pb/^{238}U$ and (b) $^{66}Zn/^{65}Cu$ ratios depending on the repetition rate employed for a 100 μm crater performed with 6 concentric circles at 0.25 mm s^{-1} and 1.5 mm s^{-1} laser beam velocity.

fractionation. Furthermore, considering the different ablation rates (from 0.1 to 10 kHz), it can be assumed that changes in the Pb/U ratio could be related to a shift of vaporisation zones for Pb within the ICP due to its higher diffusion (because smaller particles are Pb-enriched[19,55]).

As can be seen in Fig. 5b, similar trends were observed for the $^{66}Zn/^{65}Cu$ ratios. In this case the $^{66}Zn/^{65}Cu$ ratios showed a slight negative variation as a function of the repetition rate, and such deviation did not exceed 7% for both scanner speeds. In a recent study, Koch *et al.*[15] reported, for the analysis of glass SRM NIST 610 by UV-fs pulses, a decrease of the $^{66}Zn/^{65}Cu$ ratio and the $^{208}Pb/^{238}U$ ratio (in a lesser extend) with the increase of the amount of material introduced into the ICP, affecting the ICP plasma temperature and ionisation efficiency. In this case, deviations exceeding 35% were reported when the ablated mass was varied over two orders of magnitude, being such deviations attributed to plasma temperature and ionisation temperature drops due to plasma loading.

Next, the ablation rates were estimated by measuring the mass removal of the ablations operated at different repetition rates using the topography images presented in Fig. 3. Volumes ablated at different time scale for ablations performed at 0.1 kHz, 1 kHz and 10 kHz are thus presented in Table 4 and, as expected, the ablation rate increases drastically with the repetition rate. For both scanner speeds, the volume of the ablated sample after 15 s (the time period considered for the elemental ratios in this study) was roughly estimated to be in the range of 4×10^5 μm^3 at 10 kHz, 3×10^5 μm^3 at 1 kHz, and 1×10^5 μm^3 at 0.1 kHz. The $^{66}Zn/^{65}Cu$ ratio deviation observed allows estimating a plasma temperature drop of about 100–200 K. According to Koch *et al.*,[15] this four-fold mass loading increase should produce a $^{66}Zn/^{65}Cu$ drop in the range of 6%. This drop was surprisingly in good agreement with our results (<7%) taking into account the differences in operating conditions, for instance, in terms of laser pulse duration (360 fs *vs* 150 fs), laser wavelength (1030 nm *vs* 265 nm), and plasma conditions (wet *vs* dry). These results show that IR-fs-LA operated at high repetition rates (<10 kHz) and strong pulse overlapping (<99.8%) do not generate detectable preferential elemental evaporation when silicate glass samples are ablated, highlighting the limited thermal effects induced by fs pulses due to the laser-material interaction duration which is below the thermal relaxation time of the material.[56] In addition, the mass ablation rate was found to affect the $^{66}Zn/^{65}Cu$ ratio, though in a limited range under our laser ablation conditions, in good agreement with Koch *et al.*[15] using different operating conditions. This suggests that further fs-LA developments would hardly improve mass loading effects and that enhancement of the ICP robustness still needs investigation.

Table 4 Mass removal in μm^3 for ablations of 6 concentric circles repeated 2, 5 and 10 times at 0.1, 1 and 10 kHz for a scanner velocity of 0.25 mm s^{-1} and 1.5 mm s^{-1}. These ablated areas were calculated from the topography images of the crater (as shown in Fig. 3)

Volume μm^3	Time duration	0.1 kHz	1 kHz	10 kHz
Scan 0.25 mm s^{-1}				
× 2	7.76 s	39337	164116	250497
× 5	19.4 s	106296	221897	360460
× 10	38.8 s	181756	295922	415874
Scan 1.5 mm s^{-1}				
× 2	1.2 s	—	66395	276774
× 5	3.2 s	12305	153983	328286
× 10	6.4 s	37777	239049	381133

3.4. Effect of the fluence

Laser-material interaction is closely linked to the fluence, sample removal, and thermal effects being related to the energy delivered to the sample. As a consequence, the fluence is often recognized as a major parameter affecting elemental fractionation when nanosecond and femtosecond pulses are used,[15,34,57–60] and this phenomenon is emphasized when low fluences, especially close to the ablation threshold, are delivered to the sample. However it should be highlighted that opposite trends were observed under nanosecond and femtosecond ablation conditions. Cromwell and Arrowsmith[57] showed that the Zn/Cu ratio decreased with the increase of the fluence value using a 266 nm nanosecond laser,

Table 5 Ratios obtained under wet plasma conditions for all ablation strategies (based on a 15 seconds ICPMS signal)

	$^{238}U/^{232}Th$		$^{208}Pb/^{238}U$		$^{66}Zn/^{65}Cu$	
	0.25 mm s^{-1}	1.5 mm s^{-1}	0.25 mm s^{-1}	1.5 mm s^{-1}	0.25 mm s^{-1}	1.5 mm s^{-1}
25 J cm^{-2}						
0.1 kHz	1.051 ± 0.017	1.116 ± 0.019	0.481 ± 0.006	0.486 ± 0.017	0.540 ± 0.012	0.546 ± 0.014
0.3 kHz	1.015 ± 0.004	1.032 ± 0.011	0.462 ± 0.003	0.475 ± 0.004	0.540 ± 0.009	0.544 ± 0.005
1 kHz	0.970 ± 0.006	0.991 ± 0.007	0.465 ± 0.008	0.474 ± 0.006	0.532 ± 0.006	0.546 ± 0.002
5 kHz	0.999 ± 0.019	0.992 ± 0.008	0.438 ± 0.024	0.472 ± 0.005	0.508 ± 0.034	0.524 ± 0.003
14 J cm^{-2}						
0.1 kHz	1.102 ± 0.014	1.175 ± 0.018	0.486 ± 0.017	0.495 ± 0.014	0.526 ± 0.013	0.540 ± 0.008
0.3 kHz	1.027 ± 0.004	1.043 ± 0.007	0.479 ± 0.002	0.481 ± 0.007	0.537 ± 0.019	0.533 ± 0.008
1 kHz	1.040 ± 0.014	1.001 ± 0.011	0.471 ± 0.009	0.474 ± 0.002	0.522 ± 0.013	0.513 ± 0.008
5 kHz	1.044 ± 0.045	1.001 ± 0.014	0.451 ± 0.051	0.446 ± 0.005	0.508 ± 0.039	0.515 ± 0.020
10 kHz	1.078 ± 0.042	1.018 ± 0.021	0.434 ± 0.059	0.459 ± 0.022	0.492 ± 0.009	0.511 ± 0.009
5 J cm^{-2}						
0.1 kHz	1.152 ± 0.024	1.267 ± 0.100	0.489 ± 0.023	0.516 ± 0.053	0.555 ± 0.035	0.523 ± 0.023
0.3 kHz	1.068 ± 0.007	1.066 ± 0.005	0.480 ± 0.004	0.484 ± 0.007	0.514 ± 0.013	0.522 ± 0.0004
1 kHz	1.118 ± 0.023	1.018 ± 0.009	0.454 ± 0.009	0.468 ± 0.007	0.526 ± 0.034	0.493 ± 0.015
5 kHz	1.144 ± 0.034	1.092 ± 0.009	0.413 ± 0.030	0.487 ± 0.009	0.455 ± 0.031	0.542 ± 0.047
10 kHz	1.159 ± 0.030	1.055 ± 0.031	0.419 ± 0.027	0.477 ± 0.027	0.477 ± 0.034	0.576 ± 0.009

whereas the Zn/Cu ratio was found to increase with the fluence using a 266 nm femtosecond laser.[15] Moreover, in a recent study, Garcia *et al.*[60] pointed out that the elemental fractionation occurred only during the first femtosecond pulses, and the measured Zn/Cu ratio approached asymptotic values at higher shot number. The number of shots required to reach this asymptotic value are related to the fluence; the higher the fluence, the lesser the required number of shots. They proposed that the major reason for elemental fractionation in fs-LA is due to the different ionisation energies of the elements and coulomb interaction of the ions in the plasma state of matter during the ablation, without excluding thermal evaporation of volatile elements.

In order to assess the level of elemental fractionation related to the fluence when IR fs pulses are applied to glass samples at high repetition rates (*i.e.* laser ablation with a strong overlapping and high mass removal), three fluence values (5 J cm^{-2}, 14 J cm^{-2}, and 25 J cm^{-2}) were investigated taking into account the first 15 s of the analysis for each ablation (see Table 5). First, the $^{238}U/^{232}Th$ ratios were found to increase when decreasing the fluence highlighting a rising of the particle-size-related fractionation. This is likely due to the lower ablation rate provided by low fluences which constrain the laser beam to eject during a longer period of time the thicker particles related to the sample surface. In order to evaluate the impact of the fluence on the particle formation, SEM measurements of the collected laser-generated aerosols were performed at low and high fluence values. As expected, higher particle density was found at higher fluence (Fig. 6 *vs* Fig. 4). Additionally, linear aggregates were found to be larger at high fluence values likely due to higher collision probability during the particle ejection. The number of molten spherical particles was proportionally comparable from low to high fluence, and the size of molten spherical particles was also quite similar and independent of the fluence.

In contrast to the $^{238}U/^{232}Th$ ratio, the $^{66}Zn/^{65}Cu$ and $^{208}Pb/^{238}U$ ratios showed less pronounced trends as a function of the fluence. However, it is worthwhile to notice that as observed for a fluence value of 14 J cm^{-2}, both ratios decreased gradually when the ablation rate increased, confirming the mass sample loading effect reported above. Within the uncertainty of the analysis, the $^{66}Zn/^{65}Cu$ ratio was only a little higher at high fluence values, and these results are in agreement with those previously reported by Koch *et al.*[15] In such work, a 20% increase was pointed out when the fluence value was varied from 6 J cm^{-2} to 25 J cm^{-2}. However, the ablation rate and related plasma loading effects likely counterbalance the expected increase of the $^{66}Zn/^{65}Cu$ ratio as a function of fluence. Indeed,

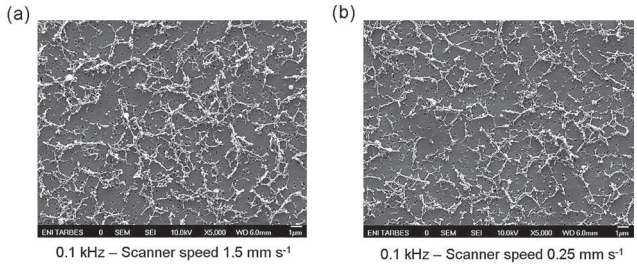

Fig. 6 SEM images of the collected aerosol produced at 0.1 kHz, 25 J cm^{-2} and scanner speed of (a) 0.25 mm s^{-1} and (b) 1.5 mm s^{-1}.

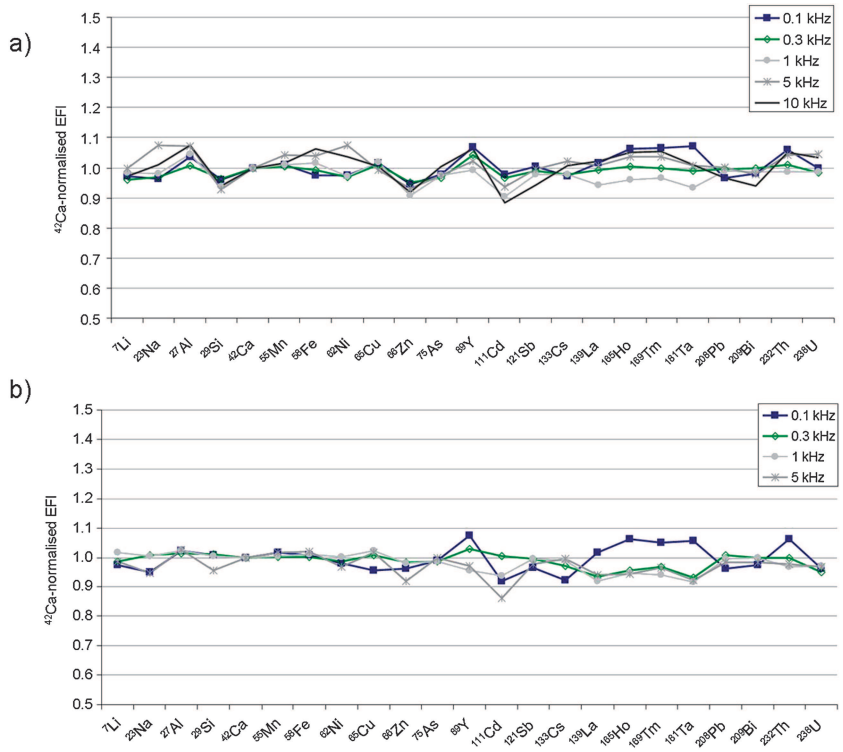

Fig. 7 Elemental Fractionation Index (EFI) normalised to ^{42}Ca, depending on laser repetition rate for a 100-μm crater obtained at 1.5 mm s^{-1} scanner speed and fluence value of (a) 14 J cm^{-2} and (b) 25 J cm^{-2}.

the mass ablated during the selected analysis interval (15 s) was estimated to be 3–4 times higher at 25 J cm^{-2} than at 5 J cm^{-2}, which was enough to attenuate the rising of the $^{66}Zn/^{65}Cu$ ratio due to different ionisation energies of the elements and coulomb interaction of the ions in the plasma state of matter during the ablation.

Finally, in order to examine the potential differences concerning elemental fractionation during the analysis of glasses by IR fs-LA-ICPMS operated at high repetition rates, the fractionation indices related to ^{42}Ca (covering a mass range from ^{7}Li up to ^{238}U) were investigated for SRM NIST 610. Fractionation in the sense of temporal drifts of elemental ratios relative to Ca as an internal standard was quantified upon the Fryer's definition modified by Koch *et al.*[15] Fig. 7a and 7b show the elemental fractionation indices (EFIs) measured by fs-LA-ICPMS for various repetition rates using two fluence values (14 J cm^{-2} and 25 J cm^{-2} respectively). EFIs were found to be in the range of 1 ± 0.05 at the high fluence regime for most of the elements whatever the repetition rate. However, more pronounced deviations were found for elemental fractionation indices at 14 J cm^{-2} compared to those obtained at 25 J cm^{-2}. Zn and Cd were systematically found to deviate to a higher extent (EFIs < 0,9), indicating a depletion of these elements during the ablation. Taking into account the analytical uncertainty, it could be stated that no specific repetition rate dependence could be pointed out, indicating that laser repetition rate is of minor importance as regards to elemental fractionation, the fluence being a more critical or influent parameter. Similar trends for elemental fractionation indices were previously reported by Koch *et al.*[15] by UV fs-LA (265 nm) of silicate glass SRM NIST 610 and therefore, the advantage of using UV wavelengths as regards to elemental fractionation is still questionable. Nevertheless, UV wavelengths certainly provide better ablation quality when highly transparent samples are ablated. For instance, the use of the experimental conditions selected in this study for fs-LA-ICPMS analysis of sapphires revealed that several cracks could occur around the ablated crater. The use of UV photons which provide more direct coupling with the material would certainly improve the ablation quality.

4. Conclusion

The elemental fractionation of a high repetition rate IR femtosecond laser ablation system was investigated for the analysis of silicate glass SRM NIST 610. Fractionation effects inherent to the ICP were minimised using wet plasma conditions which ensured more robust conditions in comparison to dry plasmas. Even with such robust conditions, particle-size-related fractionation was observed *via* $^{238}U/^{232}Th$ ratio when the sample surface was ablated. The level of fractionation was minimized by using high repetition rates or low scanner speeds due to the dilution of the large particles, coming from the sample surface, with the large amount of thinner particles, coming from deeper levels inside the sample. Additionally; the use of high repetition rates was not found to generate significant preferential evaporation of volatile element although it induces a high mass removal rate which affects ionization efficiency of the plasma (in a limited extent under the selected operating conditions). A 11% $^{208}Pb/^{238}U$ drop was however observed when the repetition rate was varied from 0.1 to 10 kHz which can not be attributed to preferential evaporation of lead during the ablation as it has been observed in nanosecond laser ablation of glass. In addition, the fluence value was found to be a major parameter affecting elemental fractionation compared to high repetition rates. In this sense, high fluence values lead to lower fractionation indices than low fluences. On the other hand, SEM measurements revealed no significant differences in the particle size and structure of the laser-generated-particles, and linear agglomerates as well as molten spherical particles were found for all ablations whatever the laser repetition rate, fluence, or scanner speed investigated.

5. Acknowledgements

The authors thank Hélène Garay, Olivier Eterradossi and Jean-Serge Bidoret (Ecole des Mines d'Alès, Pau, France) for technical support and their valuable comments during profilometer measurements. Also, Beatriz Fernández would like to acknowledge the postdoctoral fellowship from the "Secretaria de Estado de Universidades e Investigación" of the Spanish Ministry of Education and Science.

6. References

1 B. Fernandez, F. Claverie, C. Pécheyran, O. F. X. Donard and F. Claverie, *TrAC Trends in Analytical Chemistry*, 2007, **26**, 951–966.
2 J. Pisonero and D. Günther, *Mass Spectrometry Reviews*, 2008, **27**, 609–623.
3 P. M. Outridge, W. Doherty and D. C. Gregoire, *Spectrochimica Acta, Part B: Atomic Spectroscopy*, 1997, **52**, 2093–2102.
4 J. Stix, G. Gauthier and J. N. Ludden, *Canadian Mineralogist*, 1995, **33**, 435–444.
5 R. E. Russo, X. L. Mao, C. Liu and J. Gonzalez, *Journal of Analytical Atomic Spectrometry*, 2004, **19**, 1084–1089.
6 R. E. Russo, X. Mao and O. V. Borisov, *TrAC Trends in Analytical Chemistry*, 1998, **17**, 461–469.
7 J. S. Becker, *Spectrochimica Acta, Part B: Atomic Spectroscopy*, 2002, **57**, 1805–1820.
8 R. Le Harzic, N. Huot, E. Audouard, C. Jonin, P. Laporte, S. Valette, A. Fraczkiewicz and R. Fortunier, *Applied Physics Letters*, 2002, **80**, 3886.
9 C. Liu, X. L. Mao, S. S. Mao, X. Zeng, R. Greif and R. E. Russo, *Analytical Chemistry*, 2004, **76**, 379–383.
10 H. R. Kuhn and D. Günther, *Journal of Analytical Atomic Spectrometry*, 2004, **19**, 1158–1164.
11 J. Koch, A. Von Bohlen, R. Hergenröder and K. Niemax, *Journal of Analytical Atomic Spectrometry*, 2004, **19**, 267–272.
12 R. E. Russo, X. Mao, H. Liu, J. Gonzalez and S. S. Mao, *Talanta*, 2002, **57**, 425–451.
13 J. Koch, I. Feldmann, N. Jakubowski and K. Niemax, *Spectrochimica Acta, Part B: Atomic Spectroscopy*, 2002, **57**, 975–985.
14 H.-R. Kuhn, M. Guillong and D. Günther, *Analytical and Bioanalytical Chemistry*, 2004, **378**, 1069–1074.
15 J. Koch, M. Wälle, J. Pisonero and D. Günther, *Journal of Analytical Atomic Spectrometry*, 2006, **21**, 932–940.
16 J. J. Gonzalez, C. Liu, S. B. Wen, X. Mao and R. E. Russo, *Talanta*, 2007, **73**, 567–576.
17 J. J. Gonzalez, C. Liu, S. B. Wen, X. Mao and R. E. Russo, *Talanta*, 2007, **73**, 577–582.
18 H. R. Kuhn and D. Günther, *Analytical and Bioanalytical Chemistry*, 2005, **383**, 434–441.
19 J. Koch, H. Lindner, A. Von Bohlen, R. Hergenröder and K. Niemax, *Journal of Analytical Atomic Spectrometry*, 2005, **20**, 901–906.
20 M. Motelica-Heino, P. Le Coustumer and O. F. X. Donard, *Journal of Analytical Atomic Spectrometry*, 2001, **16**, 542–550.
21 C. Y. Liu, X. L. Mao, J. Gonzalez and R. E. Russo, *Journal of Analytical Atomic Spectrometry*, 2005, **20**, 200–203.

22 M. Guillong and D. Günther, *Journal of Analytical Atomic Spectrometry*, 2002, **17**, 831–837.
23 B. Hattendorf, C. Latkoczy and D. Günther, *Analytical Chemistry*, 2003, **75**, 341A–347A.
24 M. Guillong, H.-R. Kuhn and D. Günther, *Spectrochimica Acta, Part B: Atomic Spectroscopy*, 2003, **58**, 211–220.
25 A. Tunheng and T. Hirata, *Journal of Analytical Atomic Spectrometry*, 2004, **19**, 932–934.
26 R. Hergenröder, O. Samek and V. Hommes, *Mass Spectrometry Reviews*, 2006, **25**, 551–572.
27 J. Gonzalez, S. H. Dundas, C. Y. Liu, X. Mao and R. E. Russo, *Journal of Analytical Atomic Spectrometry*, 2006, **21**, 778–784.
28 J. J. Gonzalez, D. Oropeza, X. Mao and R. E. Russo, *Journal of Analytical Atomic Spectrometry*, 2008, **23**, 229–234.
29 C. Pécheyran, S. Cany and O. F. X. Donard, *Canadian Journal of Analytical Sciences and Spectrometry*, 2005, **50**, 228–239.
30 R. Freydier, F. Candaudap, F. Poitrasson, A. Arbouet, B. Chatel and B. Dupre, *Journal of Analytical Atomic Spectrometry*, 2008, **23**, 702–710.
31 M. L. Alexander, M. R. Smith, J. S. Hartman, A. Mendoza and D. W. Koppenaal, *Applied Surface Science*, 1998, **127–129**, 255–261.
32 F. Poitrasson, X. Mao, S. S. Mao, R. Freydier and R. E. Russo, *Analytical Chemistry*, 2003, **75**, 6184–6190.
33 Q. Z. Bian, J. Koch, H. Lindner, H. Berndt, R. Hergenröder and K. Niemax, *Journal of Analytical Atomic Spectrometry*, 2005, **20**, 736–740.
34 Q. Bian, C. C. Garcia, J. Koch and K. Niemax, *Journal of Analytical Atomic Spectrometry*, 2006, **21**, 187–191.
35 J. Gonzalez, C. Liu, X. Mao and R. E. Russo, *Journal of Analytical Atomic Spectrometry*, 2004, **19**, 1165–1168.
36 I. Horn and F. von Blanckenburg, *Spectrochimica Acta, Part B: Atomic Spectroscopy*, 2007, **62**, 410–422.
37 J. J. Gonzalez, A. Fernandez, D. Oropeza, X. Mao and R. E. Russo, *Spectrochimica Acta - Part B Atomic Spectroscopy*, 2008, **63**, 277–286.
38 S. M. Eggins, L. P. J. Kinsley and J. M. G. Shelley, *Applied Surface Science*, 1998, **127–129**, 278–286.
39 I. Horn, R. L. Rudnick and W. F. McDonough, *Chemical Geology*, 2000, **164**, 281–301.
40 G. Ballihaut, F. Claverie, C. Pécheyran, S. Mounicou, R. Grimaud and R. Lobinski, *Analytical Chemistry*, 2007, **79**, 6874–6880.
41 B. Fernandez, F. Claverie, C. Pécheyran and O. F. X. Donard, *Journal of Analytical Atomic Spectrometry*, 2008, **23**, 367–377.
42 B. Fernandez, F. Claverie, C. Pécheyran, J. Alexis and O. F. X. Donard, *Analytical Chemistry*, 2008, **80**, 6981–6994.
43 D. Günther and B. Hattendorf, *TrAC Trends in Analytical Chemistry*, 2005, **24**, 255–265.
44 M. Guillong, I. Horn and D. Günther, *Journal of Analytical Atomic Spectrometry*, 2003, **18**, 1224–1230.
45 C. O'Connor, B. L. Sharp and P. Evans, *Journal of Analytical Atomic Spectrometry*, 2006, **21**, 556–565.
46 D. B. Aeschliman, S. J. Bajic, D. P. Baldwin and R. S. Houk, *Journal of Analytical Atomic Spectrometry*, 2003, **18**, 1008–1014.
47 I. Novotny, J. C. Farinas, W. Jia-liang, E. Poussel and J. M. Mermet, *Spectrochimica Acta - Part B Atomic Spectroscopy*, 1996, **51**, 1517–1526.
48 G. C. Y. Chan, W. T. Chan, X. L. Mao and R. E. Russo, *Spectrochimica Acta, Part B: Atomic Spectroscopy*, 2001, **56**, 1375–1386.
49 J. F. Alder, R. M. Bombelka and G. F. Kirkbright, *Spectrochimica Acta Part B: Atomic Spectroscopy*, 1980, **35**, 163–175.
50 M. Guillong and C. A. Heinrich, *Journal of Analytical Atomic Spectrometry*, 2007, **22**, 1488–1494.
51 D. Günther and C. A. Heinrich, *Journal of Analytical Atomic Spectrometry*, 1999, **14**, 1363–1368.
52 V. Mozna, J. Pisonero, M. Hola, V. Kanicky and D. Günther, *Journal of Analytical Atomic Spectrometry*, 2006, **21**, 1194–1201.
53 H. R. Kuhn, J. Koch, R. Hergenröder, K. Niemax, M. Kalberer and D. Günther, *Journal of Analytical Atomic Spectrometry*, 2005, **20**, 894–900.
54 I. Kroslakova and D. Günther, *Journal of Analytical Atomic Spectrometry*, 2007, **22**, 51–62.
55 J. Kosler, M. Wiedenbeck, R. Wirth, J. Hovorka, P. Sylvester and J. Míková, *Journal of Analytical Atomic Spectrometry*, 2005, **20**, 402–409.
56 B. Rethfeld, K. Sokolowski-Tinten, D. Von Der Linde and S. I. Anisimov, *Applied Physics A: Materials Science and Processing*, 2004, **79**, 767–769.
57 E. F. Cromwell and P. Arrowsmith, *Analytical Chemistry*, 1995, **67**, 131–138.
58 D. Figg and M. S. Kahr, *Applied Spectroscopy*, 1997, **51**, 1185–1192.
59 X. L. Mao, A. C. Ciocan and R. E. Russo, *Applied Spectroscopy*, 1998, **52**, 913–918.
60 C. C. Garcia, H. Lindner, A. Von Bohlen, C. Vadla and K. Niemax, *Journal of Analytical Atomic Spectrometry*, 2008, **23**, 470–478.